

# Observation of superdiffusive phonon transport in aligned atomic chains

Lin Yang,<sup>1</sup> Yi Tao,<sup>1,2</sup> Yanglin Zhu,<sup>3</sup> Manira Akter,<sup>4</sup> Ke Wang,<sup>5</sup> Zhiliang Pan,<sup>1</sup> Yang Zhao,<sup>1</sup> Qian Zhang,<sup>1</sup> Yaqiong Xu,<sup>6,7</sup> Renkun Chen,<sup>8</sup> Terry T. Xu,<sup>4</sup> Yunfei Chen,<sup>2</sup> Zhiqiang Mao,<sup>3</sup> and Deyu Li<sup>1,\*</sup>

<sup>1</sup>Department of Mechanical Engineering, Vanderbilt University, Nashville, TN 14, USA.

<sup>2</sup>School of Mechanical Engineering and Jiangsu Key Laboratory for Design and Manufacture of Micro-Nano Biomedical Instruments, Southeast University, Nanjing, 210096, P. R. China.

<sup>3</sup>Department of Physics, Pennsylvania State University, University Park, PA 16802, USA.

<sup>4</sup>Department of Mechanical Engineering and Engineering Science, The University of North Carolina at Charlotte, Charlotte, North Carolina 28223, United States

<sup>5</sup>Materials Research Institute, Pennsylvania State University, University Park, PA 16802, USA

<sup>6</sup>Department of Electrical Engineering and Computer Science, Vanderbilt University, Nashville, TN 37235, USA.

<sup>7</sup>Department of Physics and Astronomy, Vanderbilt University, Nashville, TN 37235, USA.

<sup>8</sup>Department of Mechanical and Aerospace Engineering, University of California-San Diego, La Jolla, CA, 92093, USA

\*Correspondence to: [deyu.li@vanderbilt.edu](mailto:deyu.li@vanderbilt.edu).

**Superdiffusive phonon transport in one-dimensional (1D) nonlinear lattices, a direct consequence of the Fermi-Pasta-Ulam-Tsingou (FPUT) paradox<sup>1</sup>, presents a classical abnormality of continuous interest<sup>2-5</sup>. So far the concept remains purely theoretical as isolated single atomic chains of sufficient length remain unattainable in reality. Here we experimentally demonstrate superdiffusive 1D transport in van der Waals (vdW) crystal NbSe<sub>3</sub> nanowires with an unprecedented length dependence of the thermal conductivity ( $\kappa$ ) persisting over 40  $\mu\text{m}$  at room temperature and following a 1/3 power law. Interestingly, contrary to the classical size effect due to phonon-boundary scattering,  $\kappa$  shows a 25-fold enhancement as the characteristic size of the nanowires reduces from 26 to 6.8 nm while displaying a normal-superdiffusive transition. Analyses indicate that these intriguing observations stem from the transport of 1D phonons excited as a result of a record-level**

**elastic stiffening. The persistent divergent trend of the observed thermal conductivity with sample length reveals a real possibility of creating novel vdW crystal-based thermal superconductors with  $\kappa$  values higher than that of any known materials.**

Low-dimensional materials have attracted tremendous attention<sup>6-8</sup>. An important class of such materials, nanowires, are often referred to as 1D objects<sup>6</sup>; however, in most cases this designation is purely from a geometric consideration, but not in the physical sense since electrons and phonons with wave vectors along all directions are excited. In this regard, there are two distinct fundamental science problems: (i) at what diameter does a true physical dimensionality transition occur, and (ii) how does such a transition impact carrier transport? The question of what happens for phonons in 1D lattices was first numerically studied using the legendary MANIAC computer in 1955, and the unexpected outcome has been known as the classical FPUT paradox<sup>1</sup>, which suggests a divergent  $\kappa$  for 1D lattices even with nonlinear force interactions<sup>2-4</sup>. Although electron and phonon transport in 1D ballistic regime has been observed<sup>9-12</sup>, experimental demonstration of superdiffusive phonon transport in 1D lattices remains inaccessible owing to the daunting measurement challenges.

Macroscopically diffusive heat conduction is described by the phenomenological Fourier's law, linking the heat flux  $J$  to the temperature gradient  $\nabla T$  as  $J = -\kappa \nabla T$ , where  $\kappa$  is a material-intrinsic property. However, the FPUT paradox indicates recurrence of phonon modes in 1D lattices<sup>1</sup>, and the extremely slow decay of heat flux correlation leads to a divergent  $\kappa$ ,  $\sim L^\beta$  ( $0 < \beta < 1$ ), with the system size defined by its linear dimension,  $L$ . This phenomenon is also referred to as superdiffusive thermal transport<sup>2-4</sup>. To date, the actual value of  $\beta$ , a key factor in elucidating the chaotic dynamics in 1D systems, is still in debate<sup>2-5,13-15</sup>.

Several attempts have been made with the hope of recapturing the predicted superdiffusive nature of 1D phonons through exploring thermal transport in single wall carbon nanotubes

(SWCNTs)<sup>16,17</sup>. However, it has been shown that the measured  $\kappa$  becomes saturated as the tube length increases to  $\sim 10 \mu\text{m}$ <sup>16</sup>; although one recent study claimed observation of divergent  $\kappa$  for SWCNTs<sup>17</sup>, different  $\beta$  values are shown for different tubes without a physical ground, and questions have been raised about potential errors in the measurements<sup>18,19</sup>. Meanwhile, abnormal thermal transport has been predicted in  $< 3 \text{ nm}$  diameter nanowires without experimental validation<sup>20</sup>. This situation is especially frustrating as the key features of electronic devices are reaching down to  $3 \text{ nm}$ , which calls for solid experimental evidence of anomalous thermal transport in ultra-thin nanowires for precise thermal management<sup>21</sup>.

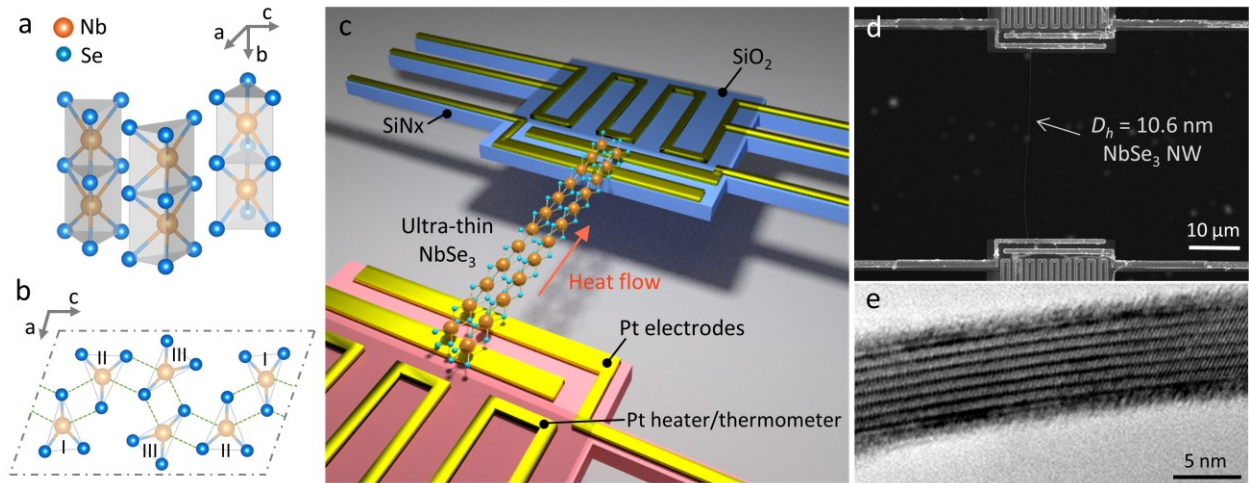


**Fig. 1. Crystalline structure of NbSe<sub>3</sub> and experimental set-up for thermal/electrical measurements.** (a) Schematic diagram showing the stacking of the prisms in NbSe<sub>3</sub>. (b) A projection of the crystal structure perpendicular to the  $b$  axis. (c) Schematic illustration of the measurement device. (d) SEM micrograph showing a nanowire on the device. (e) An HRTEM image of an ultra-thin NbSe<sub>3</sub> nanowire.

Here we report on thermal transport in vdW crystal NbSe<sub>3</sub> nanowires with a characteristic size down to  $6.8 \text{ nm}$ , and show dimensional crossover to 1D phonons with superdiffusive transport. As shown in Fig. 1a-b, NbSe<sub>3</sub> is composed of molecular chains of selenium trigonal prisms with niobium atoms residing at the center<sup>22,23</sup>. Covalently bonded 1D molecular chains assembled together *via* vdW interactions to form NbSe<sub>3</sub> nanowires, which are promising objects for revealing 1D properties<sup>22,23</sup>. High resolution transmission electron microscopy (HRTEM) study verified the

single crystalline nature of ultra-thin NbSe<sub>3</sub> nanowires (Fig. 1e), and all NbSe<sub>3</sub> nanowires prepared using liquid exfoliation method are confirmed to be oriented along the intra-chain *b* axis (Supplementary Fig. 1). The characteristic size of our nanowires is denoted by their hydraulic diameters ( $D_h$ ), four times the reciprocal of the surface-area-to-volume ratio, which better reflects the classical size effect (Supplementary Note 1).

The electrical and thermal conductivities of the NbSe<sub>3</sub> nanowires were measured using a microthermal bridge approach<sup>23–25</sup>. Fig. 1c, d show a schematic drawing and a scanning electron microscopy (SEM) image of a nanowire placed between two suspended SiN<sub>x</sub> membranes with integrated Pt heaters/resistance thermometers and extra electrodes. In the measurements, we adopted a Wheatstone bridge based differential scheme to effectively cancel the correlated temperature fluctuation to reduce the noise equivalent temperature<sup>25</sup>. A temperature resolution of ~4 mK was achieved allowing for detection of thermal conductance ( $G$ ) with a resolution of ~36 pW/K, ~1/5 of the lowest  $G$  of all measured samples (Supplementary Note 3).

Fig. 2a plots the measured room temperature  $\kappa$  versus  $D_h$ , with all nanowires having suspended lengths of ~15  $\mu\text{m}$ . Interestingly, the data indicate a clear transition at  $D_h = 26$  nm. For thicker wires,  $\kappa$  decreases as  $D_h$  reduces, as a result of boundary scattering of three dimensional (3D) phonons at nanowire surfaces<sup>23</sup>; however, as  $D_h$  further drops,  $\kappa$  demonstrates a steep upward trend. In fact, compared to the moderate reduction from 7.1 to 4.3 W/m-K as  $D_h$  decreases from 135 to 26 nm,  $\kappa$  increases by ~25 fold and reaches 109 W/m-K for a 6.8 nm diameter wire.

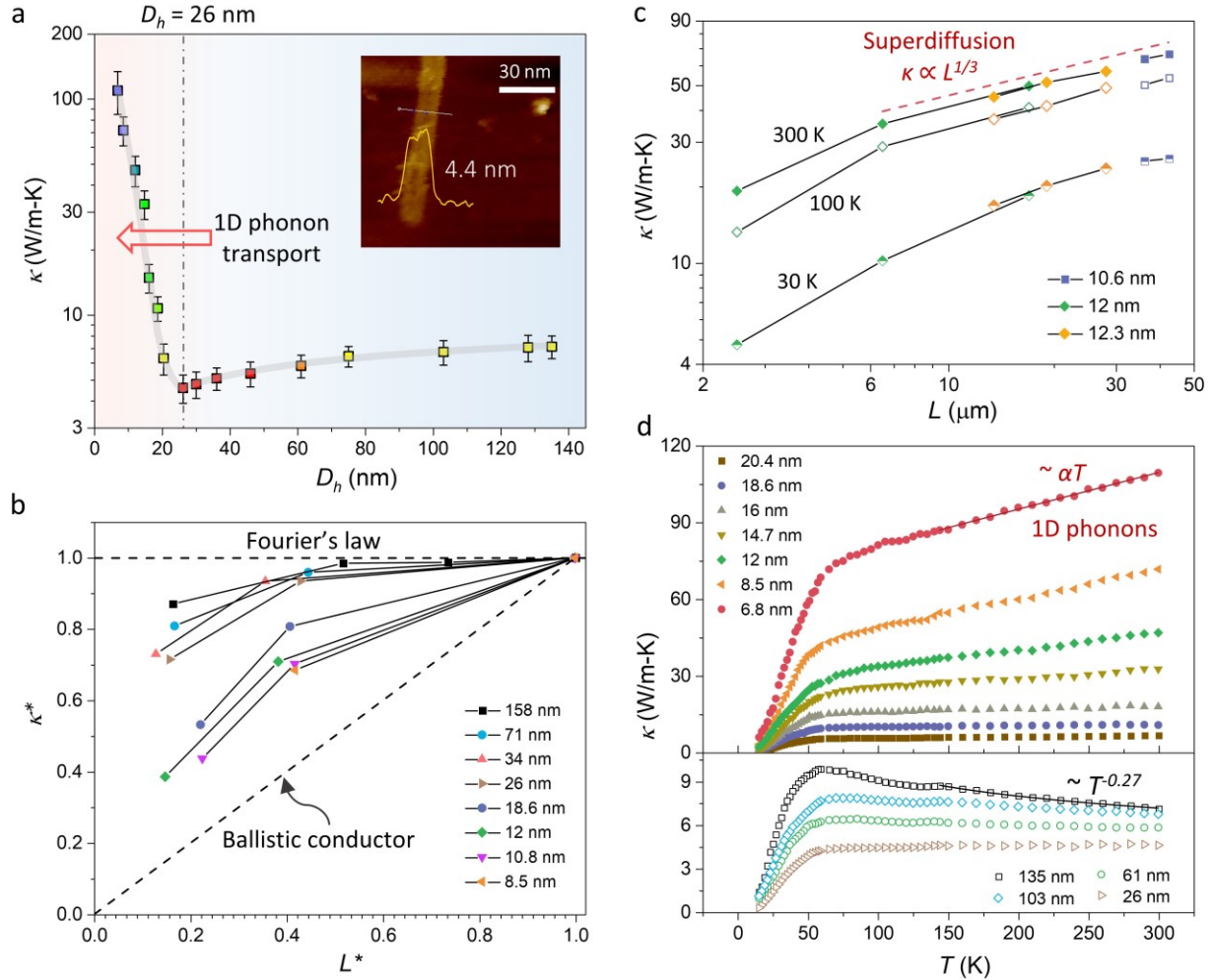


**Fig. 2. Divergent and Superdiffusive transport of 1D phonons.** (a) Measured room temperature  $\kappa$  versus  $D_h$ . The gray solid line is guide to the eyes. Inset: AFM scanning profile of the nanowire with  $D_h = 6.8$  nm. (b) Normalized room temperature  $\kappa$  versus the normalized suspended length, which indicates a normal-superdiffusive transition as the wire diameter decreases. (c) Measured  $\kappa$  versus suspended length at different temperatures (100 and 300 K) display the  $1/3$  power law divergence. Note that the deviation from the  $1/3$  power law for the measured results at 30 K is because at this temperature, the transport is not 1D phonon dominant. (d) Temperature dependence of  $\kappa$  for different diameter wires (the suspended lengths are  $\sim 15$   $\mu\text{m}$  for all samples). Thermal conductivity data in the lower panel are reprinted with permission from ref.<sup>23</sup>. Copyright 2018 American Chemical Society.

Since bulk NbSe<sub>3</sub> is a metallic compound, to understand the underlying mechanism for the observed transition, we first evaluate the electronic contribution to  $\kappa$ . The electrical resistance of NbSe<sub>3</sub> nanowires was measured using the four-probe method (Supplementary Note 7). Based on the measured electrical resistivity, we can estimate the electronic thermal conductivity,  $\kappa_e$ , using

the Wiedemann-Franz law with the Lorenz number taking the Sommerfeld value, which is a good approximation for NbSe<sub>3</sub><sup>23</sup>. We find the electrons contribute to 42% of the total  $\kappa$  for the NbSe<sub>3</sub> nanowire with  $D_h = 24$  nm at 300 K. However,  $\kappa_e$  drops rapidly as  $D_h$  reduces, and for  $D_h = 10.8$  nm, the electronic contribution is merely 3% (see Supplementary Fig. 11). As such, phonons are responsible for the drastically enhanced  $\kappa$  of ultra-thin wires.

The intriguing size-dependence prompts us to examine the length dependence of  $\kappa$ , through measuring the same nanowire with different suspended lengths (Supplementary Note 8). Fig. 2b plots the normalized room temperature thermal conductivity,  $\kappa^*$ , versus the normalized suspended length,  $L^*$ , both with respect to the values for the respective longest samples, for seven nanowires of different  $D_h$ . For meaningful comparison, the maximum length in Fig. 2b is kept  $\sim 15$   $\mu\text{m}$  (14.2–16.3  $\mu\text{m}$ ). Interestingly, for wires with large  $D_h$ ,  $\kappa$  first increases with  $L$  from  $\sim 2$  to  $\sim 6$   $\mu\text{m}$ , and then only increases marginally as  $L$  further extends, indicating that  $\kappa$  converges to a saturated value during the ballistic to diffusive transition as the wire length exceeds the phonon mean free path (MFP). However, as  $D_h$  reduces to below 26 nm,  $\kappa$  exhibits a much stronger length dependence even for  $L > 6$   $\mu\text{m}$ , suggesting a transition from diffusive to anomalous transport in the length dependence. To further explore the length dependence, we measured thinner samples with much longer suspended lengths. Fig. 2c illustrates the measured  $\kappa$  versus  $L$ , which indicates that for nanowires with  $D_h$  in the range of 10.6 to 12.3 nm, the length dependence extends beyond 40  $\mu\text{m}$  at 300 K, an unprecedented length dependence for nanowires, larger than the previously reported 8.3  $\mu\text{m}$  for SiGe wires<sup>26</sup>,  $\sim 10$   $\mu\text{m}$  for SWCNTs<sup>16</sup>,  $\sim 13$   $\mu\text{m}$  for Ta<sub>2</sub>Pd<sub>3</sub>Se<sub>8</sub> wires<sup>27</sup> and  $\sim 15$   $\mu\text{m}$  for a 25 nm diameter GaP nanowire<sup>28</sup>.

Importantly, the data in Fig. 2c indicate that in the length range of 6.5 to 42.5  $\mu\text{m}$ , the measured  $\kappa$  follows a trend of  $\kappa \propto L^\beta$ , with a constant  $\beta$  of 1/3. For phonons as major heat carriers, a divergent

$\kappa$  originates from either (i) significant ballistic phonon transport, or (ii) phonon scattering mainly through Normal process with conserved momentum. Partially ballistic transport, while renders a length dependence of  $\kappa$ , does not follow a trend of  $\kappa \propto L^\beta$  with a constant  $\beta$  over a large size range and would converge to a constant  $\kappa$  at large  $L$ , as evidenced by the thicker wires in Fig. 2b. Instead, both numerical simulations and mode coupling analyses predicted a universal  $\kappa \propto L^{1/3}$  divergence law for 1D nonlinear lattices at long chain limit<sup>3,14,15</sup> (See supplementary Note 8).

To further confirm the superdiffusive transport, we also plot the measured  $\kappa$  at 100 K in Fig. 2c, which again follows the trend of  $\kappa \propto L^{1/3}$  in the same length range. If partially ballistic phonon transport was responsible for the observed length dependence, a steeper slope would exist at 100 K as the phonon MFP is larger at lower temperature<sup>29</sup>. Thus, the consistent power law dependence at the very different  $T$  of 100 and 300 K strongly suggests the length dependence in the range of 6.5 to 42.5  $\mu\text{m}$  is due to superdiffusive behavior of 1D phonons. Note that a deviation from the 1/3 power law is shown for the measured results at 30 K, which is because at 30 K, 3D phonon modes, *i.e.*, both intra-chain and inter-chain phonons, make important contribution to thermal transport as discussed below. Therefore, no 1/3 power law length dependence is expected.

The excitation of 1D phonons in the ultra-thin nanowires is also supported by a transition in the temperature dependence of  $\kappa$ , as shown in Fig. 2d. For wires with  $D_h > 26$  nm (lower panel),  $\kappa$  decreases as  $T$  increases in the range of 50-300 K, a signature of *Umklapp* scattering. However, as  $D_h$  further reduces to below 26 nm (upper panel),  $\kappa$  starts to display an increasing trend in this high temperature regime, and a linear  $T$  dependence is observed for the measured  $\kappa$  of a 6.8 nm wire. This is drastically different from the  $T^{-2}$  dependence for the measured  $\kappa$  of SWCNTs, where *Umklapp* scattering dominates phonon transport<sup>30</sup>.

The transition to positive temperature dependence cannot be explained by changes in phonon MFP ( $l$ ) or group velocity ( $v$ ). As such, it must be due to the altered temperature dependence of heat capacity ( $C$ ) according to  $\kappa \sim Cvl$ . This transition suggests that for ultra-thin wires, the excited phonon modes must be different from those in thicker wires. The increasing  $\kappa$  with temperature suggests that more 1D phonon modes along the molecular chain are continuously populated, which can occur only if the Debye temperature,  $\theta_D$ , shifts to a higher value.  $\theta_D$  of bulk NbSe<sub>3</sub> is  $\sim 200$  K<sup>23</sup>, and since  $\theta_D \propto \sqrt{E}$ <sup>31</sup>, a higher  $\theta_D$  implies an enhanced Young's modulus ( $E$ ), a phenomenon known as elastic stiffening that occurs in various nanowires<sup>32,33</sup>.

To verify our hypothesis, we measured  $E$  of individual nanowires along the axial direction, *i.e.*,  $b$  direction, using a three-point bending scheme with an atomic force microscope (AFM).  $E$  can be extracted from the force-deflection (F-D) curve (Fig. 3a) recorded during the extension and retraction process in the bending test (see Supplementary Note 9). Fig. 3b shows that for wires with  $D_h > 40$  nm,  $E$  remains constant, and the average value of  $E = 86$  GPa is consistent with the reported bulk value<sup>34</sup>. However,  $E$  increases sharply as  $D_h$  reduces below 26 nm, reaching 423 GPa for  $D_h = 8.9$  nm, which represents a 5-fold enhancement with respect to  $E_{bulk}$ . Even though elastic stiffening has been observed in different nanowires<sup>32,33</sup>, the observed value here represents a record level of  $E$  enhancement as compared to the up to 100% enhancement for ZnO<sup>32</sup> and Ag<sup>33</sup> nanowires.

Elastic stiffening can influence the lattice thermal conductivity ( $\kappa_l$ ) in several ways. First, the enhanced  $E$  corresponds to a higher speed of sound, which is directly proportional to  $\kappa_l$ . In addition, the higher  $\theta_D$  shifts the phonon spectrum to lower wave vectors at any given  $T$ , and enlarges the bandgap between acoustic and optical phonons; both contribute to a reduced *Umklapp* scattering rate<sup>35-37</sup>. These factors all help boost  $\kappa_l$ , leading to the  $\sim 25$  fold  $\kappa$  enhancement. It is a surprise, however, that so far no experimental data or numerical results have been reported to show the

effects of elastic stiffening on phonon transport. As such, we modeled  $\kappa_l$  of bulk NbSe<sub>3</sub> with different interatomic force constants by combining first-principles calculations and Boltzmann transport equation<sup>38,39</sup> (Supplementary Note 10). In modeling bulk NbSe<sub>3</sub>, the effect of phonon-boundary scattering is neglected; this is reasonable because in ultra-thin NbSe<sub>3</sub> wires, 1D phonons along the molecular chains dominate the transport process at elevated temperatures and phonon-boundary scattering plays a marginal role. Indeed, through enhancing the interatomic force constants by six times, the modeled  $\kappa_l$  increases from 7.1 to 106.8 W/m-K at 300 K, displaying the same trend as our experimental results (Fig. 3c).

Moreover, from the calculated phonon dispersion with  $E/E_{bulk} = 6$ , the cut-off frequency,  $f_c$ , for acoustic phonon modes along the cross-chain direction is  $\sim 1.5$  THz. In contrast,  $f_c$  of along-chain acoustic phonons is  $\sim 6.5$  THz (see Supplementary Note 10). According to  $f_c = k_B T / 2\pi\hbar$ , where  $k_B$  and  $\hbar$  are the Boltzmann and Planck constant, respectively, along-chain acoustic phonons can be continuously activated as  $T$  ramps up to 312 K, while cross-chain phonon modes are fully excited at 72 K. These are all reflected in our measured results. First, as shown in Fig. 2c, both inter- and intra-chain phonons contribute to  $\kappa_l$  at 30 K, in this case the length dependence deviates from the  $L^{1/3}$  law. Moreover, the continuous excitation of high frequency 1D phonon modes in ultra-thin nanowires results in increasing  $C$  with temperature, which explains the observed positive temperature dependence in the high  $T$  regime in Fig. 2d.

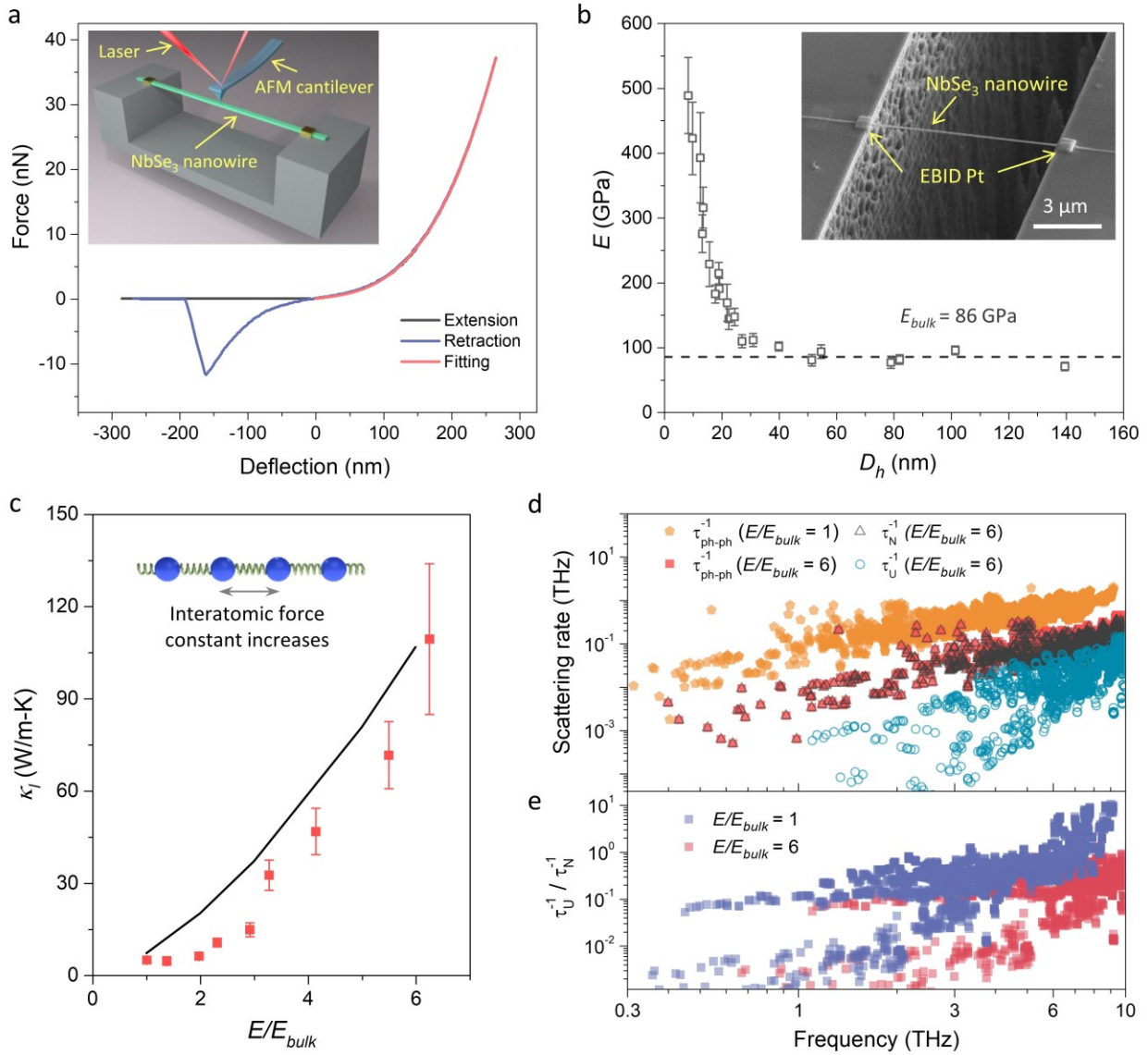


**Fig. 3. Elastic stiffening and Normal scattering dominated phonon transport.** (a) Force-deflection curves in the bending test, together with the fitting curve. Inset: schematic drawing for the bending test. (b) Measured  $E$  versus  $D_h$ , where the average bulk value is plotted as a dashed line. Inset: An SEM image of a NbSe<sub>3</sub> nanowire on top of a Si trench with electron beam induced deposition (EBID) of Pt at the two edges. (c) The modeled  $\kappa_l$  and the experimental data show the same trend as  $E$  increases. (d) Calculated total phonon-phonon scattering rate,  $\tau_{ph-ph}^{-1}$ , for two different  $E$  ratios at 300 K, where the rates of Normal,  $\tau_N^{-1}$ , and *Umklapp*,  $\tau_U^{-1}$ , scattering for  $E/E_{bulk} = 6$  are also plotted. (e) Calculated phonon mode dependent ratio of  $\tau_U^{-1}$  to  $\tau_N^{-1}$  with  $E/E_{bulk} = 1$  and 6.

To demonstrate the altered phonon scattering process, we calculated phonon mode dependent scattering rates, and separated contributions from Normal and *Umklapp* scattering as the interatomic force constant increases (Supplementary Note 10). Note that a large fraction of

*Umklapp* scattering occurs through the *acoustic + acoustic*  $\rightarrow$  *optical (aao)* process<sup>40</sup>, which becomes more difficult in ultra-thin wires as the phonon spectrum shifts to lower wave vectors and the bandgap enlarges, *i.e.*, phonon hardening effects. As shown in Fig. 3d, this reduced scattering phase space upon elastic stiffening greatly suppresses the overall three-phonon scattering rate; and moreover, Normal scattering becomes more dominant for  $E/E_{bulk} = 6$ . In fact, Fig. 3e indicates that Normal scattering strength is nearly one order of magnitude stronger than that of *Umklapp* scattering. Owing to phonon hardening, the momentum conserved Normal scattering becomes the dominant scattering process for the along-chain 1D phonons, which results in superdiffusive thermal transport for ultra-thin NbSe<sub>3</sub> nanowires.

This study presents the long-sought experimental evidence of the transition from 3D to 1D phonon transport through measuring ultra-thin NbSe<sub>3</sub> nanowires. Exotic features such as superdiffusive thermal transport with  $\kappa \propto L^{1/3}$ , 25 fold  $\kappa$  enhancement as well as normal-superdiffusive transition are observed. These changes are attributed to a record level of elastic stiffening along the molecular chain direction, which induces 1D along-chain phonons dominating thermal transport. Our discovery of divergent  $\kappa$  in vdW crystal nanowires even with perturbations due to inter-chain interactions for 1D along chain phonons calls for re-examination of the conditions for superdiffusive phonon transport. The drastically enhanced  $\kappa$  also enlightens promising approaches to manipulate phonon transport to create thermal superconductors for functional thermal devices and efficient heat dissipation.

## Online content

Any methods, additional references, Nature Research reporting summaries, source data, extended data, supplementary information, acknowledgements, peer review information; details of author contributions and competing interests; and statements of data and code availability are available.

5

1. E. Fermi, J. Pasta, and S. Ulam, Los Alamos Science Laboratory Report No. LA1940, 1955.
2. Lepri, S., Livi, R. & Politi, A. On the anomalous thermal conductivity of one-dimensional lattices. *Europhys. Lett.* **43**, 271–276 (1998).
- 10 3. Narayan, O. & Ramaswamy, S. Anomalous Heat Conduction in One-Dimensional Momentum-Conserving Systems. *Phys. Rev. Lett.* **89**, 200601 (2002).
4. Livi, R. & Lepri, S. Thermal physics: Heat in one dimension. *Nature* **421**, 327 (2003).
5. Boh, J. *Thermal Transport in Low Dimensions: From Statistical Physics to Nanoscale Heat Transfer*. (Springer Nature, 2016).
- 15 6. Xia, Y. *et al.* One-Dimensional Nanostructures: Synthesis, Characterization, and Applications. *Adv. Mater.* **15**, 353–389 (2003).
7. Zhang, Y., Tan, Y. W., Stormer, H. L. & Kim, P. Experimental observation of the quantum Hall effect and Berry’s phase in graphene. *Nature* **438**, 201–204 (2005).
8. Xu, X. *et al.* Length-dependent thermal conductivity in suspended single-layer graphene. *Nat. Commun.* **5**, 3689 (2014).
- 20 9. Bockrath, M. W. *et al.* Luttinger-liquid behaviour in carbon nanotubes. *Nature* **397**, 598–601 (1999).
10. Cui, L. *et al.* Thermal conductance of single-molecule junctions. *Nature* **572**, 628–633 (2019).
- 25 11. Cui, L. *et al.* Quantized thermal transport in single-atom junctions. *Science* **355**, 1192–1195 (2017).
12. Meier, T. *et al.* Length-dependent thermal transport along molecular chains. *Phys. Rev. Lett.* **113**, 1–5 (2014).
13. Lepri, S., Livi, R. & Politi, A. Universality of anomalous one-dimensional heat conductivity. *Phys. Rev. E - Stat. Physics, Plasmas, Fluids, Relat. Interdiscip. Top.* **68**, 8–11 (2003).
- 30 14. Wang, J. S. & Li, B. Intriguing Heat Conduction of a Chain with Transverse Motions. *Phys. Rev. Lett.* **92**, 074302 (2004).
15. Delfini, L., Lepri, S., Livi, R. & Politi, A. Anomalous kinetics and transport from 1D self-

consistent mode-coupling theory. *J. Stat. Mech. Theory Exp.* **02007**, 1742–5468 (2007).

16. Liu, J., Li, T., Hu, Y. & Zhang, X. Benchmark study of the length dependent thermal conductivity of individual suspended, pristine SWCNTs. *Nanoscale* **9**, 1496–1501 (2017).
17. Lee, V., Wu, C. H., Lou, Z. X., Lee, W. L. & Chang, C. W. Divergent and Ultrahigh Thermal Conductivity in Millimeter-Long Nanotubes. *Phys. Rev. Lett.* **118**, 135901 (2017).
18. Li, Q.-Y., Takahashi, K. & Zhang, X. Comment on ‘Divergent and Ultrahigh Thermal Conductivity in Millimeter-Long Nanotubes’. *Phys. Rev. Lett.* **119**, 179601 (2017).
19. Li, Q. Y. Response to “Reply to comment on ‘Divergent and Ultrahigh Thermal Conductivity in Millimeter-Long Nanotubes’ ”. *arXiv* (2017).
20. Zhou, Y., Zhang, X. & Hu, M. Nonmonotonic Diameter Dependence of Thermal Conductivity of Extremely Thin Si Nanowires: Competition between Hydrodynamic Phonon Flow and Boundary Scattering. *Nano Lett.* **17**, 1269–1276 (2017).
21. Pop, E. Energy dissipation and transport in nanoscale devices. *Nano Res.* **3**, 147–169 (2010).
22. Ong, N. P. & Monceau, P. Anomalous transport properties of a linear-chain metal: NbSe<sub>3</sub>. *Phys. Rev. B* **16**, 3443–3455 (1977).
23. Yang, L. *et al.* Distinct Signatures of Electron–Phonon Coupling Observed in the Lattice Thermal Conductivity of NbSe<sub>3</sub> Nanowires. *Nano Lett.* **19**, 415–421 (2019).
24. Shi, L. *et al.* Measuring thermal and thermoelectric properties of one-dimensional nanostructures using a microfabricated device. *J. Heat Transfer* **125**, 881 (2003).
25. Wingert, M. C., Chen, Z. C. Y., Kwon, S., Xiang, J. & Chen, R. Ultra-sensitive thermal conductance measurement of one-dimensional nanostructures enhanced by differential bridge. *Rev. Sci. Instrum.* **83**, 114901 (2012).
26. Hsiao, T.-K. *et al.* Observation of room-temperature ballistic thermal conduction persisting over 8.3  $\mu\text{m}$  in SiGe nanowires. *Nat. Nanotechnol.* **8**, 534–538 (2013).
27. Zhang, Q. *et al.* Thermal transport in quasi-1D van der Waals crystal Ta<sub>2</sub>Pd<sub>3</sub>Se<sub>8</sub> nanowires: size and length dependence. *ACS Nano* **12**, 2634–2642 (2018).
28. Vakulov, D. *et al.* Ballistic Phonons in Ultrathin Nanowires. *Nano Lett.* **20**, 2703–2709 (2020).
29. Mingo, N. & Broido, D. A. Length dependence of carbon nanotube thermal conductivity and the ‘problem of long waves’. *Nano Lett.* **5**, 1221–1225 (2005).
30. Pop, E., Mann, D., Wang, Q., Goodson, K. & Dai, H. Thermal conductance of an individual single-wall carbon nanotube above room temperature. *Nano Lett.* **6**, 96–100 (2006).
31. Slack, G. A. Nonmetallic crystals with high thermal conductivity. *J. Phys. Chem. Solids* **34**, 321–335 (1973).
32. Chen, C. Q., Shi, Y., Zhang, Y. S., Zhu, J. & Yan, Y. J. Size dependence of Young’s modulus in ZnO nanowires. *Phys. Rev. Lett.* **96**, 075505 (2006).

33. Cuenot, S., Frétigny, C., Demoustier-Champagne, S. & Nysten, B. Surface tension effect on the mechanical properties of nanomaterials measured by atomic force microscopy. *Phys. Rev. B* **69**, 165410 (2004).
- 5 34. Brill, J. W. & Ong, N. P. Young's modulus of NbSe<sub>3</sub>. *Solid State Commun.* **25**, 1075–1078 (1978).
35. Kang, J. S., Li, M., Wu, H., Nguyen, H. & Hu, Y. Experimental observation of high thermal conductivity in boron arsenide. *Science* **361**, 575–578 (2018).
36. Li, S. *et al.* High thermal conductivity in cubic boron arsenide crystals. *Science* **361**, 579–581 (2018).
- 10 37. Tian, F. *et al.* Unusual high thermal conductivity in boron arsenide bulk crystals. *Science* **361**, 582–585 (2018).
38. Kresse, G. & Joubert, D. From ultrasoft pseudopotentials to the projector augmented-wave method. *Phys. Rev. B* **59**, 1758–1775 (1999).
- 15 39. Li, W., Carrete, J., A. Katcho, N. & Mingo, N. ShengBTE: A solver of the Boltzmann transport equation for phonons. *Comput. Phys. Commun.* **185**, 1747–1758 (2014).
40. Lindsay, L., Broido, D. A. & Reinecke, T. L. First-principles determination of ultrahigh thermal conductivity of boron arsenide: A competitor for diamond? *Phys. Rev. Lett.* **111**, 025901 (2013).

20

## Methods

*Sample preparation for NbSe<sub>3</sub> nanowires.* Bulk NbSe<sub>3</sub> crystals were synthesized using chemical vapor transport (CVT) method as previously described<sup>23</sup>. Owing to the greatly anisotropic bonding nature, the NbSe<sub>3</sub> crystals have two easy cleavage: one parallel to the *bc* plane and the other parallel to the *ab* plane. To obtain thin NbSe<sub>3</sub> nanowires, bulk single-crystal whiskers were immersed in reagent alcohol and sonicated for 3 h, which resulted in a suspension of nanowires with various cross-sectional sizes. As shown in the HRTEM image (Fig. 1e), NbSe<sub>3</sub> nanowires obtained by this method demonstrates well-aligned molecular chains of a single crystalline nature. We finally drop-casted the suspension mixture onto a piece of polydimethylsiloxane (PDMS) and transferred individual nanowires to the microdevice with a micromanipulator for subsequent thermal and electrical properties measurements. The uniformity of the cross-section along the axial direction of the as-prepared nanowires are confirmed with cross-section examination using SEM and AFM (Supplementary Note 1).

*Thermal and electrical conductivity measurement.* We conducted the thermal and electrical measurements in a cryostat (Janis CCS-400/204) operated under a high vacuum ( $<1 \times 10^{-6}$  mbar) with a dual radiation shield configuration. Electron beam induced deposition (EBID) of the Pt/C composite was performed at the contacts between the nanowire and Pt electrodes using a dual-beam system (FIB/SEM, FEI Helios NanoLab G3) to establish good electrical contacts and minimize the contact thermal resistance (Supplementary Notes 6 and 7). Before thermal conductivity measurements at each designated temperature point, we measured the electrical resistance of NbSe<sub>3</sub> nanowire samples using the four-probe method (Supplementary Note 7). To exclude the effects from CDW sliding, we make sure the applied electric field is much smaller than the depinning threshold electrical field, and the obtained I–V curve maintains a linear shape.

For thermal conductivity measurements, a Wheatstone bridge scheme was applied at the sensing side of the measurement device to improve measurement sensitivity. The background thermal conductance between the suspended membranes was measured separately and subtracted from the measured thermal conductance of the sample. To evaluate the thermal and electrical conductivity, we obtained the exact cross-sectional area of each tested sample by cutting open the cross section using a high ion current (Supplementary Notes 1 and 2). We have confirmed that the contact thermal resistance poses negligible effects on the measured total thermal resistance, and the detailed examination on the effects of contact thermal resistance can be found in Supplementary Note 6. Besides, radiation heat loss from the nanowire to the surrounding is confirmed to be negligible (Supplementary Note 4).

*Young's modulus measurement.* The NbSe<sub>3</sub> nanowire was transferred to bridge the gap of a trench of  $\sim 7$   $\mu\text{m}$  wide etched on a silicon chip. A layer of Pt/C is locally deposited at the two ends of the ribbon through EBID to clamp the ribbon to the substrate (inset in Fig. 3b). We then measure the deflection of the wire with an AFM (Bruker Dimension Icon). Before each measurement, the sensitivity of the cantilever is calibrated by tapping it on the hard Si substrate and the spring constant is extracted through a thermal tune process. By moving and tapping the cantilever until touching the edges of the trench, we can locate its middle point. We then perform the bending test by pushing at the middle point to obtain a force-deflection (F-D) curve, as shown in Fig. 3a. The bending tests were repeated three times for each sample with reproducible results. The Young's modulus of the sample was then extracted through fitting the F-D curve using a theoretical model of a suspended elastic string with fixed ends (Supplementary Note 9).

### **Data availability**

The data supporting the findings of this study are available from the corresponding author on reasonable request.

### **Code availability**

5 The code that has been used for this work is available from the corresponding author upon reasonable request.

### **Acknowledgments**

10 The authors thank the financial support from the U.S. National Science foundation (DMR-1532107, CBET-1805924). The financial support for sample preparation was provided by the National Science Foundation through the Penn State 2D Crystal Consortium-Materials Innovation Platform (2DCC-MIP) under NSF cooperative agreement DMR-1539916. Z.Q.M. acknowledges support from the US National Science Foundation under grants DMR-1917579.

### **Author contributions**

15 L.Y. conducted transport property and Young's modulus measurements. Y.T. and L.Y. performed theoretical simulation. L.Y. and Z.P. performed sample preparation for TEM studies. Y.Z. and L.Y. fabricated wide gap suspended microdevices. Y.Z. and Z.M. synthesized the material. M.A. and K.W. performed TEM characterizations. L.Y. and D.L. compiled and analyzed results. D.L. conceived and directed the project. L.Y. and D.L. wrote the manuscript with input from all authors.

### **Competing interests**

20 Authors declare no competing interests.

### **Additional information**

Correspondence and requests for materials should be addressed to D. L.